Developmental oligodendrocytes regulate brain function through the mediation of synchronized spontaneous activity

Short title

Developmental oligodendrocytes regulate brain maturation

Authors: Ryo Masumura[1], Kyosuke Goda[1], Mariko Sekiguchi[1], Naofumi Uesaka[1]*

Affiliations:

[1]Department of Cognitive Neurobiology, Graduate School of Medical and Dental Sciences, Tokyo Medical and Dental University (TMDU), Tokyo 113-8510, Japan.

*Corresponding author & Lead Contact

Naofumi Uesaka
Email: uesaka.cnb@tmd.ac.jp

Department of Cognitive Neurobiology, Graduate School of Medical and Dental Sciences, Tokyo Medical and Dental University (TMDU), Tokyo 113-8510, Japan.

Abstract:

Synchronized spontaneous neural activity is a fundamental feature of developing central nervous systems, hypothesized to be critical for brain development. However, the mechanisms regulating this synchronization and its long-term functional implications remain poorly understood. Here, we unveil a novel role for oligodendrocytes in orchestrating synchronized spontaneous activity during a critical developmental window, with profound consequences for adult brain function. Using cell-specific genetic manipulation in the mouse cerebellum, we demonstrate that oligodendrocyte deficiency during early postnatal development, but not after weaning, disrupts the synchronization of Purkinje cell activity in both developmental and adult stages. These early disruption of oligodendrocytes and neural synchrony resulted in persistent alterations in adult cerebellar-dependent behaviors, including anxiety, sociality, and motor function. Our findings establish a causal link between developmental oligodendrocyte-regulated neural synchrony and the emergence of complex brain functions. This study ensures the proper developmental trajectory necessary for driving brain function and opens new avenues for understanding neurodevelopmental disorders.

Introduction

The early ability of immature animals to respond to environmental stimuli and produce various outputs, even before sensory inputs become fully active, suggests the pre-organization of complex neural networks. This organization is underpinned by robust developmental processes, with spontaneous activity emerging as a key driver in shaping neural circuits. During early postnatal development, spontaneous activity is highly correlated across neural populations in various species and systems (Kirkby *et al.*, 2013; Ackman & Crair, 2014). The widespread occurrence of the correlated spontaneous activity suggests a fundamental and universal principle driving brain maturation, where the activity can facilitate the establishment of precise sensory maps and extensive neural networks required for sensory information processing and outputs.

In the developing central nervous system, correlated spontaneous activity initially manifests as synchronized patterns in localized or extensive regions (Adelsberger *et al.*, 2005; Good *et al.*, 2017; Babola *et al.*, 2018; Mizuno *et al.*, 2018; Murakami *et al.*, 2022; Fujimoto *et al.*, 2023). Synchronized patterns then transition to desynchronized states as seen in the cortex, cerebellum, and olfactory bulb (Good *et al.*, 2017; Mizuno *et al.*, 2018; Fujimoto *et al.*, 2023). Despite the recognition of these patterns, the mechanisms governing the synchronized patterns and these roles remain elusive. One intriguing hypothesis of the mechanisms is the involvement of glial cells which play essential roles in supporting and modulating neuronal functions. Among glial cells, oligodendrocytes stand out as potential regulators of synchronized spontaneous activity due to their involvement in myelination and regulation of conduction velocity (Pajevic *et al.*, 2014; Pajevic *et al.*, 2023). The process of myelin formation continues throughout life, but the majority of myelin formation is

concentrated during postnatal development in many brain regions (de Faria *et al.*, 2021). However, the roles of oligodendrocytes in brain maturation remain largely unknown.

We tried to elucidate the causality among developmental oligodendrocytes, synchronized spontaneous activity, and brain function in the developing mouse cerebellum. To examine the causality, we focused on the mouse cerebellum since the developmental process of synchronized spontaneous activity is well known (Good *et al.*, 2017). To manipulate developmental oligodendrocytes, we employed an adeno-associated virus (AAV) vector with high specificity to oligodendrocytes, enabling precise spatiotemporal reduction of these cells in the developing mouse cerebellum. We found that the reduction of oligodendrocytes during the second to third postnatal week disrupted synchronized activity of Purkinje cells. Behavioral assessments further demonstrate that these developmental perturbations of oligodendrocytes and synchronized activity translate into significant impairments in adult cerebellar function, evidenced by anxiety-like behaviors, diminished social interactions, and impaired motor coordination. These results suggest that oligodendrocytes are a key orchestrator of synchronized spontaneous activity, crucial for the typical development of brain function.

Materials and methods

Experimental animals

This study was conducted under the recommendations of the Regulations for Animal Experiments and Related Activities at Tokyo Medical and Dental University. All animal experiment was approved by the Committees on Gene Recombination Experiments and Animal Experiments of Tokyo Medical and Dental University. All animals were group housed and maintained on a 12hr:12hr light dark cycle. All efforts were made to reduce the number of animals used and to minimize the suffering and pain of animals. WT mice (C57BL6N, 6 days -16 weeks, Sankyo labo service) were used in this study.

Plasmids.

The human MAG gene promoter sequences were amplified by PCR from human genomic DNA using primer pairs (Table. 1) and inserted into sites of hSyn promoter in AAV-U6-sgRNA-hSyn-mCherry (a gift from Alex Hewitt, Addgene plasmid # 87916) (AAV-hMAG-mcherry). hSyn promoter was removed by ApaI and BaMH1. The promoter was cloned using the Gibson Cloning Assembly Kit (New England BioLabs) following standard procedures. For AAV-hMAG-DTA, we amplified the DTA coding sequence from the pAAV-mCherry-flex-dtA (a gift from Naoshige Uchida, Addgene plasmid # 58536) using primer pairs (Table. 1) and cloned it into AAV-MAG-mcherry. The sequences of jGCaMP7f gene and jGCaMP7s were amplified by PCR from pGP-AAV-syn-jGCaMP7f-WPRE and pGP-AAV-syn-jGCaMP7s-WPRE (a gift from Douglas Kim & GENIE Project, Addgene plasmid #104488 and #104487) and inserted into sites of GFP in pAAV/L7-6-GFP-WPRE (a gift from Hirokazu Hirai, Addgene plasmid # 126462) (pAAV-L7-6-jGCaMP7f and pAAV-L7-6-jGCaMP7s) and into sites of GFP in pAAV-TRE-EGFP (a gift from Hyungbae Kwon, Addgene plasmid # 89875) (pAAV-TRE-jGCaMP7f and pAAV-TRe-jGCaMP7s). For AAV-TRE-Kir2.1-T2A-GFP, we amplified the sequences of Kir2.1-T2A-GFP from the pAAV hSyn FLEx-loxp Kir2.1-2A-GFP (a gift from Kevin Beier & Robert Malenka, Addgene plasmid # 161574), and cloned it into sites of GFP in pAAV-TRE-EGFP. For AAV-TRE-jGCaMP7f-T2A-Kir2.1, we amplified the sequences of jGCaMP7f and Kir2.1 from the pGP-AAV-syn-jGCaMP7f-WPRE and pAAV hSyn FLEx-loxp Kir2.1-2A-GFP, and cloned it into sites of GFP in pAAV-TRE-EGFP.

AAV packaging and injection.

The AAVs were produced using standard production methods. HEK293 cells were transfected with by Polyethylenimine. AAV9, PHPeB (Chan *et al.*, 2017) and Olig001 (Powell *et al.*, 2016) were used. Virus was collected after 120 h from both cell lysates and media. Purification Kit (Takara) was used for viral particle purification. All batches produced were in the range 10^{10} to 10^{11} viral genomes per milliliter. The procedure for viral vector injection has been modified from the previous lentivirus protocol(Uesaka *et al.*, 2014). 1-1.5 µL of viral solution were injected into the cerebellum of C57BL/6N mice at 100 nl / min.

Immunohistochemistry.

Mice were perfused with 4% paraformaldehyde in 0.1 M phosphate buffer, and processed for parasagittal microslicer sections (100 µm in thickness). After permeabilization and blockade of nonspecific binding, the following antibodies were applied for 2 days at 4 ^{o}C: an antibody against Car8 (Car8-GP-Af500 or Car8-Go-Af780, diluted 1:300, Nittobo Medical) to visualize PCs; an antibody against S100b (S100b-GP-Af630, 1:300, Nittobo Medical); an antibody against Iba (Wako 019-19741, 1:1000), an antibody against RFP (390004, 1:1000, Synaptic Systems or PM005, 1:500, MBL), an antibody against MBP (NBP2-50035, 1:1000, Novus), an antibody against ASPA (ABN16986, 1:1000, Merck), an antibody against vGluT2 (MSFR106290, 1:300, Nittobo Medical), and/or an antibody against GFP (#06083-05, 1:1000, Nacalai Tesque). After incubation with secondary antibodies (an anti-rat Alexa Fluor 488, an anti-guinea pig Cy3, an anti-goat Alexa Fluor 488, an anti-goat Alexa Fluor 647, an anti-mouse Cy5, an anti-rabbit Cy3, an anti-rabbit Alexa Fluor 488), the immunolabeled sections were washed and then examined under a fluorescent microscope (BZ-X700 or BZ-X800, Keyence).

In vivo calcium imaging.

Animals were put on a warm blanket and anesthetized with a mixture of midazolam (4 mg/kg body weight (BW)), butorphanol (5 mg/kg BW), and medetomidine (0.3 mg/kg BW). The depth of anesthesia was constantly monitored by observing pinch-induced

forelimb withdrawal reflex. The skin and muscles over the skull were removed and a metal plate was fixed with dental acrylic cement over the lobule 5-7 of the cerebellar vermis. A craniotomy of 3 mm diameter was made and the dura mater was carefully removed. A sterile circular 3mm diameter glass coverslip (#CS01078 3mm diameter, Matsunami) was put directly on the dura mater and was secured in place with surgical adhesive (Alon-Alpha A, Sankyo). A custom-made metal headplate with a 5 mm circular imaging well was fixed to the skull over the cranial window with dental cement (Super-Bond, Sun-medical, Japan). The head of the mouse was immobilized by attaching the head plate to a custom-made stage. We then administered atipamezole (0.3mg/kg, anti-sedan) (100 μg/g of body weight, intraperitoneal injection) for anesthesia reversal. After a 10 - 15 minutes waiting period, in vivo calcium imaging was performed using an Olympus MVX10 fluorescence microscope or a two-photon microscope (Nikon, AX R MP) equipped with a ×16 objective lens (Nikon, CFI75 LWD 16X W) and an ultrafast laser (Axon 920-2 TPC). During the recordings, the animals were lied on a warm blanket to keep the body temperature at 37°C. Laser power for the two-photon microscope was maintained <20 mW at the sample. Images were obtained in a 2D plane (2048 x 2048 pixels) using Andor SOLIS software (Oxford Instruments, frame rate 5 Hz) or in a 2D plane (512 × 512 pixels) using Nikon NIS-Elements software (frame rate, 1 Hz) for the two photon microscope. Data were saved as TIFF files.

We resized raw calcium imaging videos (TIFF format) to a resolution of 512 x 512 pixels with a 8-bit depth using ImageJ (JAVA-based processing program, USA). We cropped out the unwanted areas. Regions of interest (ROIs) corresponding to the active PC dendrites were detected using the Suite2p software (Marius Pachitariu, GitHub). This software executed a two-dimensional phase-correlation-based non-rigid image registration in the XY plane, extracted the ROIs considered as PC dendrites, and calculated the fluorescence intensity changes in each ROI. We exported these data as MAT files. The MAT files were imported into MATLAB R2023b (MathWorks, USA) for further analysis using custom-made MATLAB routines. The fluorescence intensity (F) was converted to ΔF/F0 wave, expressed as ΔF/F0 = (F - F0)/(F0), where F0 is the baseline fluorescence in the absence of calcium transients. F0 was defined as follows. First, we calculated a threshold as mean + 1 SD of the F wave of each ROI, and then the

F wave below the threshold was averaged to obtain F0. Parameters such as amplitude, frequency, half-width, and area of each calcium transient were quantified by the custom-made MATLAB routines. The correlation coefficient among all ROI pairs was calculated as previously described (Tsutsumi *et al.*, 2015). The resulting correlation matrix captured relationships among all ROI pairs in the dataset.

Behaviors.

Male mice from 2 to 3 months of age 6-7 days after AAV injection were used for behavioral tests. Before the experiments, the mice were habituated in the testing areas for at least 30 min. Mice behavior was recorded through the video camera set in the experimental room. The open field test was performed in a 50 cm x 50 cm x 40 cm (W x D x H) open field box for 10 min. Total distance mice traveled and the time in the center and peripheral regions were automatically analyzed by the ImageJ software (MouBeAT) (Bello-Arroyo *et al.*, 2018).

The sociality test was performed in the open field apparatus (50 x 50 x 40 cm, W x D x H). The test consisted of a 10-min habituation session and a 10-min test session. In the habituation session, mice were allowed to explore the open field freely. In the test session, two quadrangular cages with slits (8 cm x 8 cm, 18 cm high) were placed in two adjacent corners. One cage contained a novel mouse (8-week-old male C57BL6N) and the other was a mouse doll, and a test mouse was first placed in the outer regions of open field arena at the longest distance from these cages. The times spent around the two cages areas (12 cm in diameter) were analyzed automatically with the ImageJ software (MouBeAT). Social preference was assessed by the following equation: Sociality index = $(T_{mouse})/(T_{doll})$ where T_{mouse} and T_{doll} are the staying time around the mouse cage and that around the doll cage, respectively.

To assess motor coordination and motor learning, mice were subjected to a rotarod test. Mice were placed on a resting state rotarod (model LE8205, Panlab) for three consecutive days with two trials per day spaced 10 min apart (30 min and 40 min after CNO injection). For each trial, the rotarod was accelerated linearly from 4 rpm to 40 rpm over 300 s. Latency to fall from the start of rotation was measured.

Statistical analysis

All data are presented as mean ± SEM. Statistical significance was assessed by Mann-Whitney U test for the comparison of two independent samples. To compare the two different categorical independent samples on one dependent variable, Two-way ANOVA with post-hoc test (Bonferroni correction) was used as indicated in the text. Statistical analysis was conducted with GraphPad Prism program. Differences between groups were judged to be significant when p values were smaller than 0.05. *, **, ***, **** and ns represents $p < 0.05$, $p < 0.01$, $p < 0.001$, $p < 0.0001$ and not significant, respectively.

Results

Developmental oligodendrocytes regulate synchronized spontaneous activity

To elucidate the role of oligodendrocytes in the regulation of synchronized spontaneous activity, we engineered an oligodendrocyte-specific adeno-associated virus (OL-AAV) characterized by a human myelin associated glycoprotein (hMAG) promoter and an oligodendrocyte directional capsid, and employed it for a genetic approach to developmental oligodendrocytes (Figure 1A). We focused on the developing mouse cerebellum in which synchronized spontaneous activity and its transition were observed during postnatal development (Good *et al.*, 2017; Kano *et al.*, 2018). Mature oligodendrocytes and myelination appeared in the cerebellum during postnatal day 5 (P5) to P7 (Figure supplement 1A-B). Injection of OL-AAVs expressing mCherry into the cerebellum of P7 mice resulted in selective expression of mCherry in cerebellar oligodendrocytes at P21 (>98%) (Figure 1B-D). Injection of OL-AAVs expressing Diphtheria toxin A (DTA) into the cerebellum of postnatal day 7 (P7) mice resulted in a significant reduction of oligodendrocytes and myelination by P10 and P14, with the recovery of the number of oligodendrocytes and the extent of myelination observed by P21 and in adulthood (Figure 1E-F and figure supplement 1C-D). This temporal pattern of oligodendrocyte reduction allowed us to specifically assess the role of these cells during a critical window of cerebellar development.

We tested whether oligodendrocyte deficit affected synchronized spontaneous activity in the cerebellar Purkinje cell (PC) population. PCs show synchronized spontaneous activity in response to climbing fiber synaptic inputs in newborn mice and exhibit progressive desynchronization as development progresses (Good *et al.*, 2017). In vivo calcium imaging of PCs revealed a marked reduction in synchrony of spontaneous

activity among PCs at P13-15 following oligodendrocyte reduction (Figure 2A-D). This effect was observed across both proximal and distal PC populations (Figure 2E-F), indicating a widespread disruption of neural activity synchronization. Notably, other parameters such as frequency, amplitude, and area of calcium transients remained unchanged (Figure 2G-I), suggesting a specific effect on PC activity synchrony rather than general neural activity. We examined the effect of oligodendrocyte reduction on PC activity synchrony in earlier developmental stage (P10-11). We found that the oligodendrocyte reduction by the injection of OL-AAVs DTA at P7 led to a significant reduction in PC activity synchrony without alterations in other neural activity parameters at P10-11 (Figure supplement S2). These findings collectively demonstrate a crucial role for developmental oligodendrocytes in regulating synchronized spontaneous activity in the developing cerebellum.

Developmental oligodendrocyte affects brain function

We explored whether oligodendrocytes and synchronized spontaneous activity during cerebellar development affect adult brain function. We first investigated the long-term effects of oligodendrocyte reduction during cerebellar development on the synchrony of Purkinje cell (PC) activity in the adult cerebellum. We selectively ablated oligodendrocytes in the cerebellum of early postnatal mice and monitored the subsequent effects on PC activity as the animals matured. Our results demonstrated that the developmental reduction of oligodendrocytes leads to persistent hyposynchrony of PC activity into adulthood, while other parameters of PC activity remain unaffected (Figure 3). This result raises the possibility that developmental disturbances in

oligodendrocyte function could have lasting impacts on brain function and highlights the importance of developmental oligodendrocytes in maintaining the synchrony of neuronal activity throughout life. The cerebellum plays a crucial role in sensory-motor functions, including chewing, postural control, tone, movement, the coordination of balance, eye movements, and reflexes (Stoodley & Schmahmann, 2018; Algin *et al.*, 2023). Additionally, the cerebellum is involved in cognitive, social, and emotional coordination (Schmahmann, 2019; Van Overwalle *et al.*, 2020). Researches have also highlighted the potential role of the cerebellum in mental states, extending beyond its traditional association with motor control (Depping *et al.*, 2018). To examine roles of developmental oligodendrocytes in these brain function, we injected OL-AAVs with hMAG-mCherry or hMAG-DTA at P6-7 into distinct compartments (left, center, right) of the cerebellum (Figure S3), aligning with the cerebellum's functional segmentation (Manni & Petrosini, 2004; Guell *et al.*, 2018). Behavioral assessments in adulthood unveiled that oligodendrocyte reduction in the cerebellum during development precipitates anxiety-like behavior specifically when targeted to the central cerebellar region, but did not affect distance travelled, underscoring the compartment-specific role in anxiety regulation (Figure 4A-C). Additionally, across all regions, mice with oligodendrocyte reduction during development exhibited diminished sociality and impaired motor coordination, evidenced by reduced social approach to novel mouse and decreased latency to fall in the Rotarod test, respectively (Figur 4D-G). These data indicate that developmental oligodendrocytes are essential for mental states, sociality, and motor function in adult stages.

Developmental oligodendrocytes during specific time windows affect each brain function

We next examined a critical period for oligodendrocyte influence on cerebellar function and a link between developmental oligodendrocytes and cerebellar function. We administrated hMAG-DTA to the central cerebellum at postnatal week 3 (3W_DTA mice), when mice are weaned. Oligodendrocytes in the cerebellum of mice injected by hMAG-DTA were significantly reduced at 4 weeks (1 week after AAV injection) compared with control mice with only hMAG-mCherry, but were returned to the number similar to control mice at 2 months old (Figure 5A-C), indicating a temporary effect of the ablation. Calcium imaging analysis of 3W_DTA mice at 4weeks old revealed the reduction in the amplitude and area of PC calcium transients, but not in frequency and correlation coefficient (Figure 5D-J). This data suggest that oligodendrocytes before and after the weaning of mice play distinct roles in PC activity. Behavioral assessments in adulthood of these mice uncovered no significant behavioral anomalies in anxiety or sociality (Figure 5K-O). However, the mice injected by hMAG-DTA showed a deficit in motor learning or peak performance as evidenced by diminished performance at day3 in the Rotarod test (Figure 5P). These data suggest that oligodendrocytes before and after weaning exert distinct effects on neural activity and brain function.

Synchronized spontaneous activity during development regulates brain functions

To directly clarify a causal link between synchronized PC activity during developmental stage and cerebellar function, we employed a novel experimental strategy involving the selective manipulation of CF activity which induces PC calcium transients. We manipulated the synchronized spontaneous activity of PC population through the expression of Kir2.1, a potassium channel known to reduce neuronal excitability, in a subset of CFs whose synaptic inputs induce calcium transients in PCs (Hashimoto *et al.*, 2011; Good *et al.*, 2017). The co-injection of AAVs with EGFP or Kir2.1-T2A-GFP under the control of TRE promoter and AAVs with tetracycline transactivator (tTA) under the control of Htr5b promoter (Dorgans *et al.*, 2022) into the mouse inferior olivary nucleus at P7 resulted in a subset of CFs being labeled with EGFP in the cerebellum at P22 (Figure 6A-C). We confirmed by in vivo calcium imaging of CFs that activity of CFs with Kir2.1-T2A-jGCaMP7 was lower than that for CFs with only jGCaMP7 at P13-15 (Figure supplement 4A-D). In vivo calcium imaging of PC population revealed that the synchrony of spontaneous activity of PC population with a subset of CFs which expressed Kir2.1 was lower than that for control mice at P13-15 (Figure 6D-H). The frequency and area of calcium transients were not altered by Kir2.1 expression in a subset of CFs (Figure 6I and 6K). The amplitude of calcium transients tended to be lower in Kir2.1 expressing mice than that for control mice ($p = 0.065$, Figure 6J). These results indicate that kir2.1 expression in a subset of CFs leads to reduced synchrony of PC population activity.

We analyzed behaviors at 2 months old for mice expressing Kir2.1 in a subset of CFs from developmental stage (injection of AAVs with Kir2.1 at P7). Distance

travelled and percentage time spent in center in kir2.1-expressing mice from the developmental stage tented to decrease compared with those for control, though not statistically significant (Figure 6L-N). We further found that kir2.1-expressing mice from the developmental stage exhibited diminished sociality and impaired motor coordination, evidenced by reduced social approach to novel mouse and decreased latency to fall in the Rotarod test, respectively (Figure 6O-Q). Those results indicate that the behavioral consequences of ablating oligodendrocytes during development are similar to those of reducing synchrony during development. Together, our comprehensive analyses reveal a pivotal role for oligodendrocytes during developmental critical periods, affecting cerebellar function through mechanisms involving synchronized spontaneous activity.

Discussion

This study provides compelling evidence that oligodendrocytes play a crucial role beyond their traditional functions in myelination, extending to the regulation of synchronized spontaneous activity, and emphasizing the complexity of glial-neuronal interactions in the developing brain. Moreover, our research illuminates the significance of brain development following a proper course in brain function integrity

In adult brain, adaptive myelination can induce and maintains synchrony of spontaneous activity among neural populations (Kato *et al.*, 2020; Bonetto *et al.*, 2021; Pajevic *et al.*, 2023). Developmental oligodendrocytes have been also speculated to regulate the synchrony of neuronal activities (Jang *et al.*, 2019) . Our present study directly demonstrate that developmental oligodendrocytes regulate the synchrony of neuronal spontaneous activity. Myelin formation and plasticity modulates axonal conduction velocity, while signals from neurons are known to induce myelination (Fields, 2015). The modulation of axonal conduction velocity through oligodendrocyte-neuron interactions may result in synchrony of spontaneous activity among neuronal populations during development, and changes in these interactions may cause desynchronization.

Oligodendrocytes and oligodendrocyte precursor cells (OPCs) play crucial roles in the central nervous system, with functions extending beyond myelination. Recent research has begun to unravel their complex involvement in synapse function (Wilton *et al.*, 2019; Liu *et al.*, 2023). Notably, OPCs have been implicated in synapse elimination, a critical process in neural circuit refinement (Yamazaki *et al.*, 2019; Auguste *et al.*, 2022). In the cerebellum, synapse elimination at CF-PC synapses occurs from the first to the third postnatal week (Kano *et al.*, 2018). Intriguingly, this

timeframe coincides with the development of oligodendrocytes in the region. Our study demonstrates that oligodendrocyte reduction after the third postnatal week does not affect locomotor activity, anxiety, and sociality, suggesting the presence of a critical developmental window for oligodendrocyte influence on these brain functions. Previous researches have linked abnormal synapse elimination to various neurodevelopmental disorders, including autism spectrum disorders and schizophrenia (Penzes *et al.*, 2011). Given the temporal correlation between oligodendrocyte development and synapse elimination, the relationship between synapse elimination and brain diseases, and our findings that oligodendrocytes during the process of synapse elimination are essential for brain functions, we suggest that oligodendrocyte-mediated synapse elimination may be a key mechanism underlying certain aspects of brain function and dysfunction.

Correlated spontaneous activity have been shown to play a pivotal role in neural development and the establishment of functional neural circuits especially in the developing visual system (Kirkby *et al.*, 2013; Ackman & Crair, 2014). Retinal waves observed in various species, play a fundamental role in developing interconnections within the visual system including topographic maps. Recent study demonstrates that retinal wave not merely random but possesses an intrinsic directionality that prefig the optic flow patterns encountered after eye opening. However, the effects of correlated spontaneous activity during development on brain functionalization remain largely unknown. Our study suggests that synchronized spontaneous activity during development play a crucial role in the subsequent brain functionalization, potentially through the mediation of synapse development. These studies provide new insights into specific information content carried by correlated spontaneous activity and their influence on the development of brain functions including higher-order function,

extending beyond the previously understood role of these activity in neural circuit maturation.

There is growing evidence that oligodendrocytes and myelin affect learning, memory, and cognitive function (de Faria *et al.*, 2021; Munyeshyaka & Fields, 2022). Moreover, numerous studies have reported the changes of white matter, oligodendrocyte, and myelin in schizophrenia, autism spectrum disorders, depression, and anxiety, suggesting that the deficit of oligodendrocytes and myelin may underlie multiple brain disorders (Edgar & Sibille, 2012; de Faria *et al.*, 2021). However, it is unclear when, where, and how oligodendrocytes and myelin are involved in the functionalization of brain and the pathogenesis of these brain disorders. Our data that synchronized spontaneous activity during development controlled by oligodendrocytes is a precursor to the maturation of functional neural circuits and brain functions provides a novel lens through which to examine the etiology of disorders characterized by synaptic imbalances and dysregulation of neural activity. Thus, oligodendrocyte and myelination abnormalities, and the resulting disruption of correlated activity in neuronal populations, may be new therapeutic targets for multiple brain disorders.

Given the pivotal role of oligodendrocytes in neural circuit maturation, future research should aim to further dissect the molecular and cellular mechanisms underpinning their influence on synchronized spontaneous activity. Understanding the signaling pathways and interaction networks involved could open new therapeutic avenues for addressing developmental brain disorders and enhancing neural repair after injury.

Acknowledgments:

We thank Dr. Daisuke Tanaka, Dr. Shizuki Inaba, Dr. Ayaka Nakai, and other lab members of Uesaka lab for helpful comments and discussions.

Funding:

This work is supported by MEXT Grants-in-Aid for Scientific Research on transformative research area B “Design-build of brain through spontaneous brain multimodal activity” (KAKENHI 22H05092, 22H05093), the Asahi Glass Foundation, Toray Foundation, Takeda Science Foundation, Tokumori Yasumoto Memorial Trust, and Uehara Memorial Foundation to N.U.

Author contributions:

Initiation and conceptualization: N.U. Investigation: R.M., K.G., M.S., and N.U. Writing - original draft: N.U. Writing - editing: R.M., K.G., N.U., with inputs from all authors. Visualization: R.M., and N.U. Supervision: N.U. Funding acquisition: N.U.

Competing interests: The authors declare no conflicts of interest.

Data and materials availability: All data are available in the main text or the supplementary materials.

Materials availability

All unique/stable reagents generated in this study are available from the lead contact upon request with a completed Materials Transfer Agreement.

Data and code availability

Requests for behavioral and/or calcium imaging data reported in this paper will be shared by the lead contact upon reasonable request.

Any additional information required to reanalyze the data reported in this paper is available from the lead contact upon reasonable request.

References

Ackman, J.B. & Crair, M.C. (2014) Role of emergent neural activity in visual map development. *Current opinion in neurobiology*, **24**, 166-175.

Adelsberger, H., Garaschuk, O. & Konnerth, A. (2005) Cortical calcium waves in resting newborn mice. *Nat Neurosci*, **8**, 988-990.

Algin, O., Kocak, O.M., Gokcekuyu, Y. & Turker, K.S. (2023) Demonstration of chewing-related areas in the brain via functional magnetic resonance imaging. *Pol J Radiol*, **88**, e65-e74.

Auguste, Y.S.S., Ferro, A., Kahng, J.A., Xavier, A.M., Dixon, J.R., Vrudhula, U., Nichitiu, A.S., Rosado, D., Wee, T.L., Pedmale, U.V. & Cheadle, L. (2022) Oligodendrocyte precursor cells engulf synapses during circuit remodeling in mice. *Nat Neurosci*, **25**, 1273-1278.

Babola, T.A., Li, S., Gribizis, A., Lee, B.J., Issa, J.B., Wang, H.C., Crair, M.C. & Bergles, D.E. (2018) Homeostatic Control of Spontaneous Activity in the Developing Auditory System. *Neuron*, **99**, 511-524 e515.

Bello-Arroyo, E., Roque, H., Marcos, A., Orihuel, J., Higuera-Matas, A., Desco, M., Caiolfa, V.R., Ambrosio, E., Lara-Pezzi, E. & Gomez-Gaviro, M.V. (2018) MouBeAT: A New and Open Toolbox for Guided Analysis of Behavioral Tests in Mice. *Front Behav Neurosci*, **12**, 201.

Bonetto, G., Belin, D. & Karadottir, R.T. (2021) Myelin: A gatekeeper of activity-dependent circuit plasticity? *Science*, **374**, eaba6905.

Chan, K.Y., Jang, M.J., Yoo, B.B., Greenbaum, A., Ravi, N., Wu, W.L., Sanchez-Guardado, L., Lois, C., Mazmanian, S.K., Deverman, B.E. & Gradinaru, V. (2017) Engineered AAVs for efficient noninvasive gene delivery to the central and peripheral nervous systems. *Nat Neurosci*, **20**, 1172-1179.

de Faria, O., Jr., Pivonkova, H., Varga, B., Timmler, S., Evans, K.A. & Karadottir, R.T. (2021) Periods of synchronized myelin changes shape brain function and plasticity. *Nat Neurosci*, **24**, 1508-1521.

Depping, M.S., Schmitgen, M.M., Kubera, K.M. & Wolf, R.C. (2018) Cerebellar Contributions to Major Depression. *Front Psychiatry*, **9**, 634.

Dorgans, K., Guo, D., Kurima, K., Wickens, J. & Uusisaari, M.Y. (2022) Designing AAV Vectors for Monitoring the Subtle Calcium Fluctuations of Inferior Olive Network in vivo. *Front Cell Neurosci*, **16**, 825056.

Edgar, N. & Sibille, E. (2012) A putative functional role for oligodendrocytes in mood regulation. *Transl Psychiatry*, **2**, e109.

Fields, R.D. (2015) A new mechanism of nervous system plasticity: activity-dependent myelination. *Nature reviews. Neuroscience*, **16**, 756-767.

Fujimoto, S., Leiwe, M.N., Aihara, S., Sakaguchi, R., Muroyama, Y., Kobayakawa, R., Kobayakawa, K., Saito, T. & Imai, T. (2023) Activity-dependent local protection and lateral inhibition control synaptic competition in developing mitral cells in mice. *Dev Cell*, **58**, 1221-1236 e1227.

Good, J.M., Mahoney, M., Miyazaki, T., Tanaka, K.F., Sakimura, K., Watanabe, M., Kitamura, K. & Kano, M. (2017) Maturation of Cerebellar Purkinje Cell Population Activity during Postnatal Refinement of Climbing Fiber Network. *Cell Rep*, **21**, 2066-2073.

Guell, X., Schmahmann, J.D., Gabrieli, J. & Ghosh, S.S. (2018) Functional gradients of the cerebellum. *Elife*, **7**.

Hashimoto, K., Tsujita, M., Miyazaki, T., Kitamura, K., Yamazaki, M., Shin, H.S., Watanabe, M., Sakimura, K. & Kano, M. (2011) Postsynaptic P/Q-type Ca2+ channel in Purkinje cell mediates synaptic competition and elimination in developing cerebellum. *Proc Natl Acad Sci U S A*, **108**, 9987-9992.

Jang, M., Gould, E., Xu, J., Kim, E.J. & Kim, J.H. (2019) Oligodendrocytes regulate presynaptic properties and neurotransmission through BDNF signaling in the mouse brainstem. *Elife*, **8**.

Kano, M., Watanabe, T., Uesaka, N. & Watanabe, M. (2018) Multiple Phases of Climbing Fiber Synapse Elimination in the Developing Cerebellum. *Cerebellum*, **17**, 722-734.

Kato, D., Wake, H., Lee, P.R., Tachibana, Y., Ono, R., Sugio, S., Tsuji, Y., Tanaka, Y.H., Tanaka, Y.R., Masamizu, Y., Hira, R., Moorhouse, A.J., Tamamaki, N., Ikenaka, K., Matsukawa, N., Fields, R.D., Nabekura, J. & Matsuzaki, M. (2020) Motor learning requires myelination to reduce asynchrony and spontaneity in neural activity. *Glia*, **68**, 193-210.

Kirkby, L.A., Sack, G.S., Firl, A. & Feller, M.B. (2013) A role for correlated spontaneous activity in the assembly of neural circuits. *Neuron*, **80**, 1129-1144.

Liu, Y., Shen, X., Zhang, Y., Zheng, X., Cepeda, C., Wang, Y., Duan, S. & Tong, X. (2023) Interactions of glial cells with neuronal synapses, from astrocytes to microglia and oligodendrocyte lineage cells. *Glia*, **71**, 1383-1401.

Manni, E. & Petrosini, L. (2004) A century of cerebellar somatotopy: a debated representation. *Nature reviews. Neuroscience*, **5**, 241-249.

Mizuno, H., Ikezoe, K., Nakazawa, S., Sato, T., Kitamura, K. & Iwasato, T. (2018) Patchwork-Type Spontaneous Activity in Neonatal Barrel Cortex Layer 4 Transmitted via Thalamocortical Projections. *Cell Rep*, **22**, 123-135.

Munyeshyaka, M. & Fields, R.D. (2022) Oligodendroglia are emerging players in several forms of learning and memory. *Commun Biol*, **5**, 1148.

Murakami, T., Matsui, T., Uemura, M. & Ohki, K. (2022) Modular strategy for development of the hierarchical visual network in mice. *Nature*, **608**, 578-585.

Pajevic, S., Basser, P.J. & Fields, R.D. (2014) Role of myelin plasticity in oscillations and synchrony of neuronal activity. *Neuroscience*, **276**, 135-147.

Pajevic, S., Plenz, D., Basser, P.J. & Fields, R.D. (2023) Oligodendrocyte-mediated myelin plasticity and its role in neural synchronization. *Elife*, **12**.

Penzes, P., Cahill, M.E., Jones, K.A., VanLeeuwen, J.E. & Woolfrey, K.M. (2011) Dendritic spine pathology in neuropsychiatric disorders. *Nat Neurosci*, **14**, 285-293.

Powell, S.K., Khan, N., Parker, C.L., Samulski, R.J., Matsushima, G., Gray, S.J. & McCown, T.J. (2016) Characterization of a novel adeno-associated viral vector with preferential oligodendrocyte tropism. *Gene Ther*, **23**, 807-814.

Schmahmann, J.D. (2019) The cerebellum and cognition. *Neurosci Lett*, **688**, 62-75.

Stoodley, C.J. & Schmahmann, J.D. (2018) Functional topography of the human cerebellum. *Handb Clin Neurol*, **154**, 59-70.

Tsutsumi, S., Yamazaki, M., Miyazaki, T., Watanabe, M., Sakimura, K., Kano, M. & Kitamura, K. (2015) Structure-function relationships between aldolase C/zebrin II expression and complex spike synchrony in the cerebellum. *J Neurosci*, **35**, 843-852.

Uesaka, N., Uchigashima, M., Mikuni, T., Nakazawa, T., Nakao, H., Hirai, H., Aiba, A., Watanabe, M. & Kano, M. (2014) Retrograde semaphorin signaling regulates synapse elimination in the developing mouse brain. *Science*, **344**, 1020-1023.

Van Overwalle, F., Manto, M., Cattaneo, Z., Clausi, S., Ferrari, C., Gabrieli, J.D.E., Guell, X., Heleven, E., Lupo, M., Ma, Q., Michelutti, M., Olivito, G., Pu, M., Rice, L.C., Schmahmann, J.D., Siciliano, L., Sokolov, A.A., Stoodley, C.J., van Dun, K., Vandervert, L. & Leggio, M. (2020) Consensus Paper: Cerebellum and Social Cognition. *Cerebellum*, **19**, 833-868.

Wilton, D.K., Dissing-Olesen, L. & Stevens, B. (2019) Neuron-Glia Signaling in Synapse Elimination. *Annu Rev Neurosci*, **42**, 107-127.

Yamazaki, Y., Abe, Y., Shibata, S., Shindo, T., Fujii, S., Ikenaka, K. & Tanaka, K.F. (2019) Region- and Cell Type-Specific Facilitation of Synaptic Function at Destination Synapses Induced by Oligodendrocyte Depolarization. *J Neurosci*, **39**, 4036-4050.

Figure captions

Figure 1 | DTA expression by oligodendrocyte-specific AAVs deletes oligodendrocytes in the mouse cerebellum during the specific developmental period.

A, Diagram illustrating the injection of AAV-hMAG-mCherry and AAV-hMAG-DTA into the mouse cerebellum at early postnatal days (P6-7). **B**, Fluorescence microscopy image showing mCherry expression (red) in the section of cerebellum at P14 following AAV-hMAG-mCherry injection at P7. Scale bar, 300 µm. **C**, Specificity of mCherry expression (red) in ASPA-positive oligodendrocytes (green) at P14 by AAV-hMAG-mCherry injection at P7. Scale bar, 100 µm. **D**, Scatter plot graph depicting the percentage of RFP and ASPA double-positive cells among RFP-positive populations (from 2 mice). **E**, Sequential visualization of oligodendrocyte reduction over time, indicated by ASPA staining in cerebellar sections from control (AAV-hMAG-mCherry) and DTA-treated (AAV-hMAG-DTA) mice at P10, P14, P21, and P78. Scale bar, 100 µm. **F**, Quantification of ASPA-positive cell density at each stage (from 3 mice per group per each stage). Bars and dots indicate mean and data from individual fields of view, respectively. **** $p < 0.0001$ (Mann-Whitney U test).

Figure 2 | Oligodendrocyte reduction by oligodendrocyte-specific AAVs reduces the synchrony of PC population activity during mouse cerebellar development.

A, Diagram illustrating the time course of AAV injection (P7) and calcium imaging (P13-P15) in control and DTA-expressing mice with jGCaMP7f expression in the PCs. **B**, Schema of in vivo calcium imaging and representative one frame of full-frame scan movie recorded in lobule VI/VII of the cerebellum of control mouse at P14. Scale bar = 0.5 mm. **C-F**, Decrease in correlation coefficients (CCs) indicating reduced synchrony of spontaneous activities among PC population at P13-15 following DTA-mediated oligodendrocyte ablation. **C**, Representative time-course of spontaneous calcium transients by extracting relative fluorescence changes by in vivo calcium imaging captured from 25 regions of interest (ROIs) in the cerebellum of control and DTA-expressing mice at P14. Scale bar = 20 s. Y-axis is $\Delta F/F0 = (F - F0)/(F0)$. **D**, Correlation coefficient matrices for spontaneous calcium transient activity across multiple ROIs in CTL (upper panel) and DTA (lower panel) mice, with the color scale indicating the strength of the correlation between pairs of ROIs. **E**, Mean correlation coefficients between calcium traces from pairs of ROIs plotted against the distance of separation between pairs of ROIs in control (n = 4 mice) and AAV-hMAG-DTA-injected (n = 4 mice) mice. Error bars indicate SEM. **F**, Scatter plot graph of CCs for ROI pairs, categorized by separation distances of 0–80

mm and 120–200 mm (analyzed from four mice per group). Lines and plots indicate mean and data from individual separation distances, respectively. **G-I**, Quantification of the frequency, amplitude, and integrated area of calcium transients in control (AAV-hMAG-mCherry) and DTA-treated (AAV-hMAG-DTA) mice at P13-15 (data from four mice per group). Bars and dots indicate mean and data from individual ROIs, respectively. **** $p < 0.0001$ (Mann-Whitney U test).

Figure 3 | Oligodendrocyte ablation during postnatal development diminishes neuronal synchrony at adult stage.

A, Representative traces of spontaneous calcium transients from 25 regions of interest (ROIs) in control (CTL, top) and AAV-hMAG-DTA-injected (DTA, bottom) mice, illustrating changes in synchrony. **B,** Correlation matrices for spontaneous calcium transients comparing CTL (upper) and DTA (lower) mice, with correlation strength indicated by color intensity. **C,** Scatter plots of correlation coefficients for ROI pairs within short (0-80µm) and long (120-200µm) distances in control and DTA mice, showing significant reductions in the DTA group. **D,** Line graph showing the correlation coefficient as a function of inter-ROI distance, with CTL (orange) and DTA (cyan) mice displaying differing correlation coefficient profiles. **E-G,** Bar graphs comparing the mean of frequency (E), amplitude (F), and integrated area (G) of fluorescence transients in CTL and DTA mice. Each graph includes individual data points for each ROI. Statistical significance in panels e and g is indicated by asterisks (**** $p < 0.0001$, Mann-Whitney U tests).

Figure 4 | Oligodendrocyte reduction during development leads to behavioral abnormalities.

A-C, Assessment of exploratory behavior and locomotor activity in control (CTL, orange) and DTA-injected (DTA, cyan) mice in a novel environment, with trajectories of mouse exploratory behavior (**A**), distance traveled (**B**), and time spent in center (**C**) for mice with the injection of AAVs into distinct compartments (left, center, right) of the cerebellum (LCH, CBV, RCH). Bars and dots indicate mean and data from individual mice, respectively. **D-F,** Representative images and quantitative analysis of sociality in CTL and DTA mice with the injection of AAVs into distinct compartments (LCH, CBV, RCH). Diagram in (**D**) shows the method of sociality test; (**E**) displays the heatmap of mouse exploratory behavior, and (**F**) shows the mean

percentage of time spent around strange mouse with data points representing individual mice. **G,** Line graph showing mean latency to fall in the rotarod test over a three-day period for CTL and DTA mice, with separate graphs for mice with the injection of AAVs into distinct compartments (LCH, CBV, RCH). Error bars indicate SEM. Error bars indicate SEM. Statistical significance is indicated by asterisks (*$p < 0.05$, **$p < 0.01$, *** $p < 0.001$, **** $p < 0.0001$, Mann-Whitney U tests).

Figure 5 | Oligodendrocyte reduction after 3 weeks old in mice does not affect PC activity synchrony and mouse behaviors except for motor learning.

A, B, Fluorescence microscopy images comparing ASPA expression in the cerebellum of control (CTL) and 3-week DTA-treated (3W_DTA) mice at 4 weeks (**A**) and 8 weeks (**B**) old. ASPA-positive oligodendrocytes appear in pink. Scale bar, 50µm. **C,** Quantification of the number of ASPA-positive cells per mm^2 in the cerebellum of CTL and 3W_DTA mice at 4 and 8 weeks old, with data points for each field of view overlaid on the bar graphs (mean). **D,** Representative calcium imaging traces from PCs in the cerebellar cortex of control (CTL) and 3-week DTA-treated (3W_DTA) mice at 4weeks old, showing 25 regions of interest (ROIs). **E,** Correlation coefficient matrices of calcium transients between ROIs from CTL and 3W_DTA mice, indicating the level of synchrony, with warmer colors representing higher correlation coefficients. **F,** Line graph depicting mean correlation coefficients with increasing inter-ROI distance for CTL and 3W_DTA mice. Error bars indicate SEM. **G,** Scatter plot comparing the correlation coefficients of calcium transients in PCs between adjacent ROIs in CTL and 3W_DTA mice. **H-J,** Bar graphs displaying mean frequency (**H**), amplitude (**I**), and area (**J**) of fluorescence calcium transients for CTL and 3W_DTA mice, with significant differences denoted by asterisks. Data points represent individual ROIs. **K-M,** Assessment of exploratory behavior and locomotor activity in control (CTL, orange) and 3 weeks DTA-injected (3W_DTA, cyan) mice in a novel environment, with trajectories of mouse exploratory behavior (**F**), distance traveled (**G**), and time spent in center (**H**). **N, O**, Representative images and quantitative analysis of sociality in CTL and 3W_DTA mice. **N** displays the heatmap of mouse exploratory behavior, and (**O**) shows the mean percentage of time spent around strange mouse with data points representing individual mice. **P,** Line graph showing mean latency to fall in the rotarod test over a three-day period for CTL and 3W_DTA mice. Error bars show

SEM. Statistical significance is indicated by asterisks (**p < 0.01, **** p < 0.0001, Mann-Whitney U tests).

Figure6. | Kir2.1 expression in CFs reduces the synchrony of PC population spontaneous activity and leads to abnormal behaviors similar to the phenotype of mice with developmental oligodendrocyte reduction.

A, Fluorescent images of sagittal cerebellar sections showing Car8 immunoreactivity (Purkinje cells, magenta) and GFP expression (Climbing fibers (CFs), green). Scale bar, 200 µm. **B,** Higher magnification of the boxed area in **A** showing detailed GFP-labeled CF morphology. Scale bar, 100 µm. **C,** Scatter plot graph depicting the percentage of PCs with GFP-positive CFs among PC populations (17 sections from 10 mice). **D**, Schematic timeline of AAV injection at P7 and Ca^{2+} imaging with jGCaMP7 at P13-15 for the CTL and Kir2.1 groups. **E,** Representative time-course of spontaneous calcium transients from regions of interest (ROIs) in the mouse cerebellum at P13 showing spontaneous PC activity in control mice (CTL, top) and mice expressing Kir2.1 in a subset of CFs (kir2.1, bottom). Scale bar, 20 s. Y-axis is $\Delta F/F0 = (F - F0)/(F0)$. **F,** Correlation matrices for spontaneous PC activity between ROIs in control (top) and kir2.1-expressing (bottom) mice. The color scale indicates correlation strength. **G**, Graph displaying the correlation coefficient of Ca^{2+} transients among PCs as a function of distance between adjacent PCs in CTL and Kir2.1 groups. Data points indicate the mean ± SEM. **H,** Scatter plot comparing correlation coefficients for ROI pairs within 0-80µm and 120-200µm separation distance ranges in CTL (orange) and kir2.1-expressing (cyan) mice at P13-15, with lines representing average values. **I-K**, Bar graphs showing the comparison between CTL and Kir2.1-overexpressing CFs in terms of (**I**) frequency, (J) amplitude, and (**K**) area under the curve of Ca^{2+} transients. Data are presented as mean. Each graph includes individual data points for each ROI. **L-N,** Analysis of exploratory behavior and locomotor activity in CTL (orange) and Kir2.1-expressing (green) mice with distance traveled (**L, M**) and percentage of time spent in the center (**N**) in an open-field test. **O, P,** Representative images and quantitative analysis of sociality in CTL and Kir2.1-expressing mice. (**O**) displays the heatmap of mouse exploratory behavior, and (**P**) shows the percentage of time spent around strange mouse. **Q**, Rotarod test. The line graph shows the mean latency to fall across three days for CTL and Kir2.1-expressing mice. Error bars indicate SEM. Statistical significance is indicated by asterisks (**p < 0.01, *** p < 0.001, Mann-Whitney U tests).

Fig.1

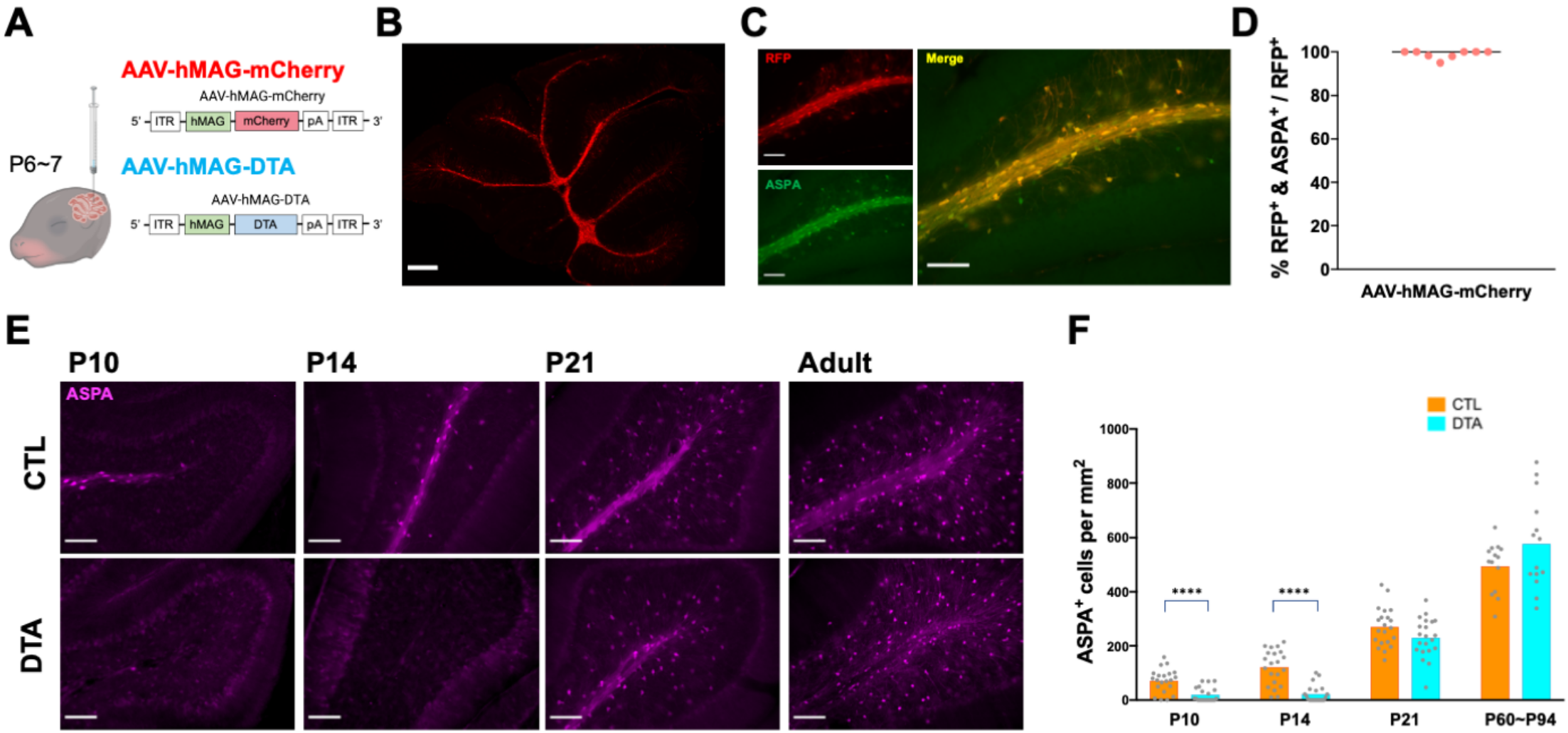
A
AAV-hMAG-mCherry
AAV-hMAG-mCherry
5' ITR hMAG mCherry pA ITR 3'
P6~7
AAV-hMAG-DTA
AAV-hMAG-DTA
5' ITR hMAG DTA pA ITR 3'
B
C
RFP
ASPA
Merge
D
% RFP+ & ASPA+ / RFP+
100
80
60
40
20
0
AAV-hMAG-mCherry
E
P10
P14
P21
Adult
ASPA
CTL
DTA
F
CTL
DTA
ASPA+ cells per mm2
1000
800
600
400
200
0
****
****
P10
P14
P21
P60~P94

Fig.2

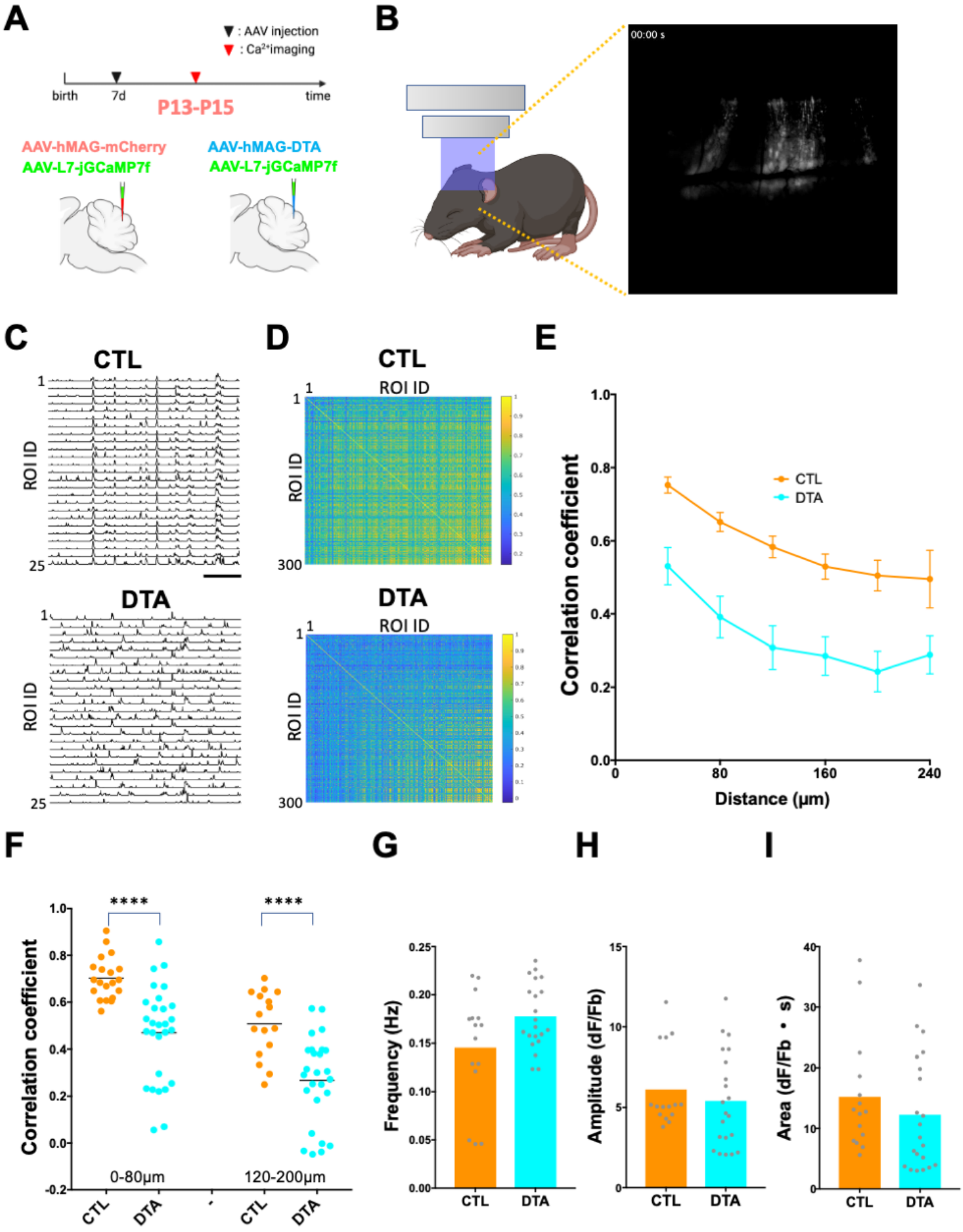
A
▼ : AAV injection
▼ : Ca2+imaging
birth
7d
time
P13-P15
AAV-hMAG-mCherry
AAV-L7-jGCaMP7f
AAV-hMAG-DTA
AAV-L7-jGCaMP7f
B
00:00 s
C
CTL
ROI ID
1
25
DTA
ROI ID
1
25
D
CTL
ROI ID
1
300
DTA
ROI ID
1
300
E
Correlation coefficient
Distance (μm)
CTL
DTA
0
80
160
240
F
Correlation coefficient
****
****
0-80μm
120-200μm
CTL
DTA
CTL
DTA
G
Frequency (Hz)
CTL
DTA
H
Amplitude (dF/Fb)
CTL
DTA
I
Area (dF/Fb • s)
CTL
DTA

Fig. 3

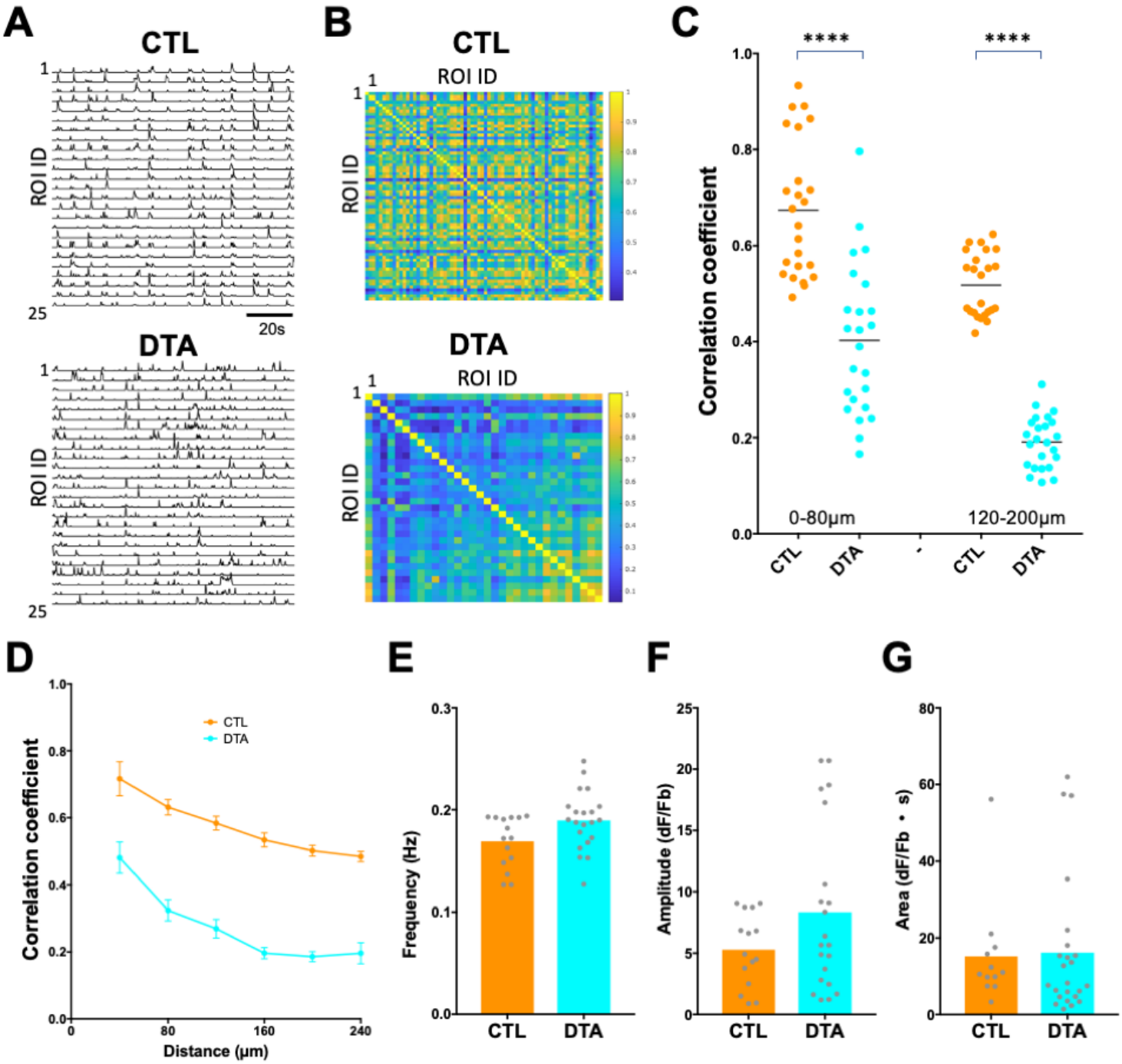
A
CTL
ROI ID
1
25
20s
DTA
B
CTL
ROI ID
DTA
C
Correlation coefficient
****
****
0-80μm
120-200μm
CTL
DTA
D
Correlation coefficient
Distance (μm)
CTL
DTA
E
Frequency (Hz)
F
Amplitude (dF/Fb)
G
Area (dF/Fb • s)

Fig. 4

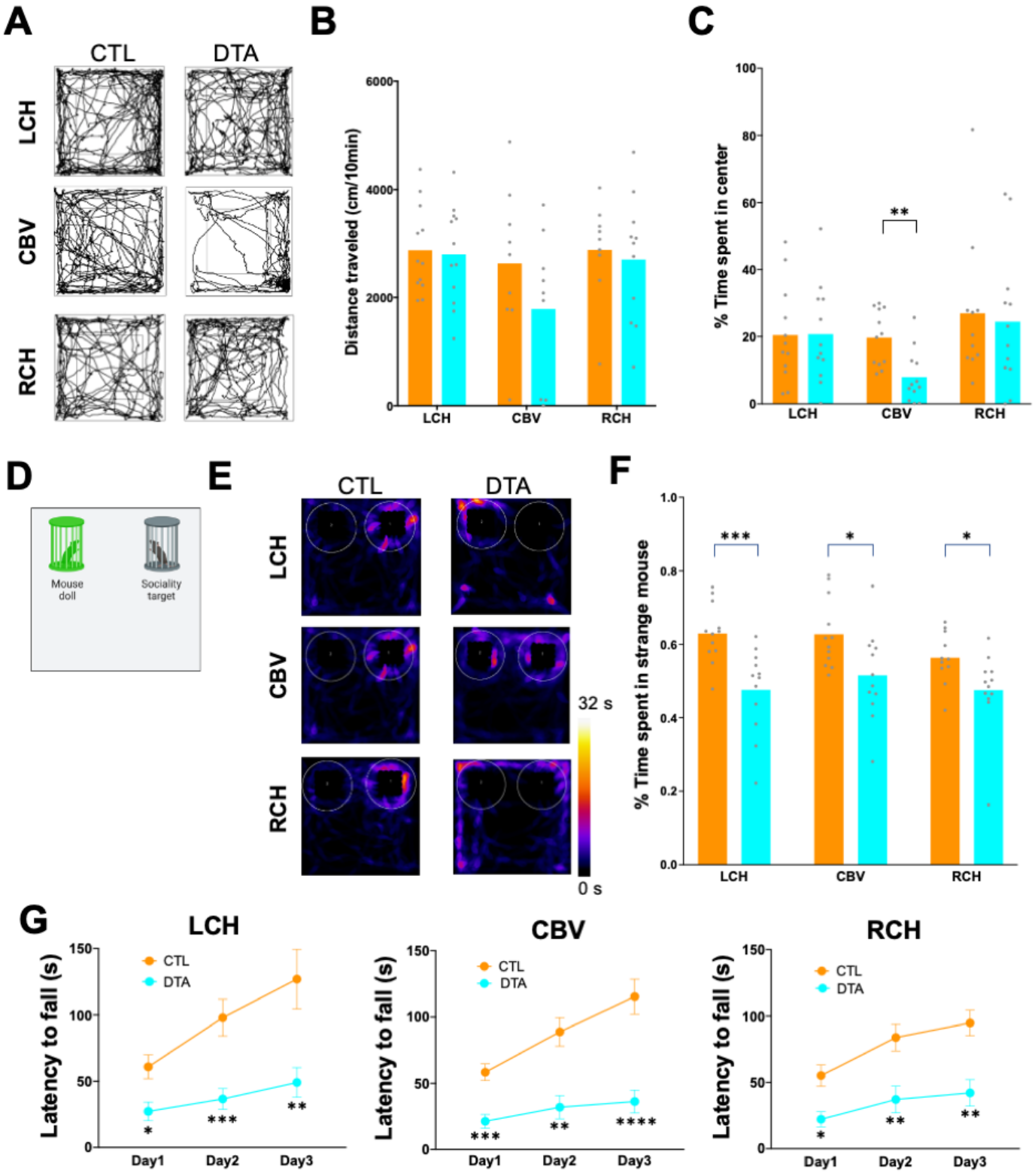
A
CTL
DTA
LCH
CBV
RCH
B
Distance traveled (cm/10min)
6000
4000
2000
0
LCH
CBV
RCH
C
% Time spent in center
100
80
60
40
20
0
**
LCH
CBV
RCH
D
Mouse doll
Sociality target
E
CTL
DTA
LCH
CBV
RCH
32 s
0 s
F
% Time spent in strange mouse
1.0
0.8
0.6
0.4
0.2
0.0
***
*
*
LCH
CBV
RCH
G
LCH
CBV
RCH
Latency to fall (s)
150
100
50
0
CTL
DTA
*
***
**
***
**
****
*
**
**
Day1
Day2
Day3

Fig.5

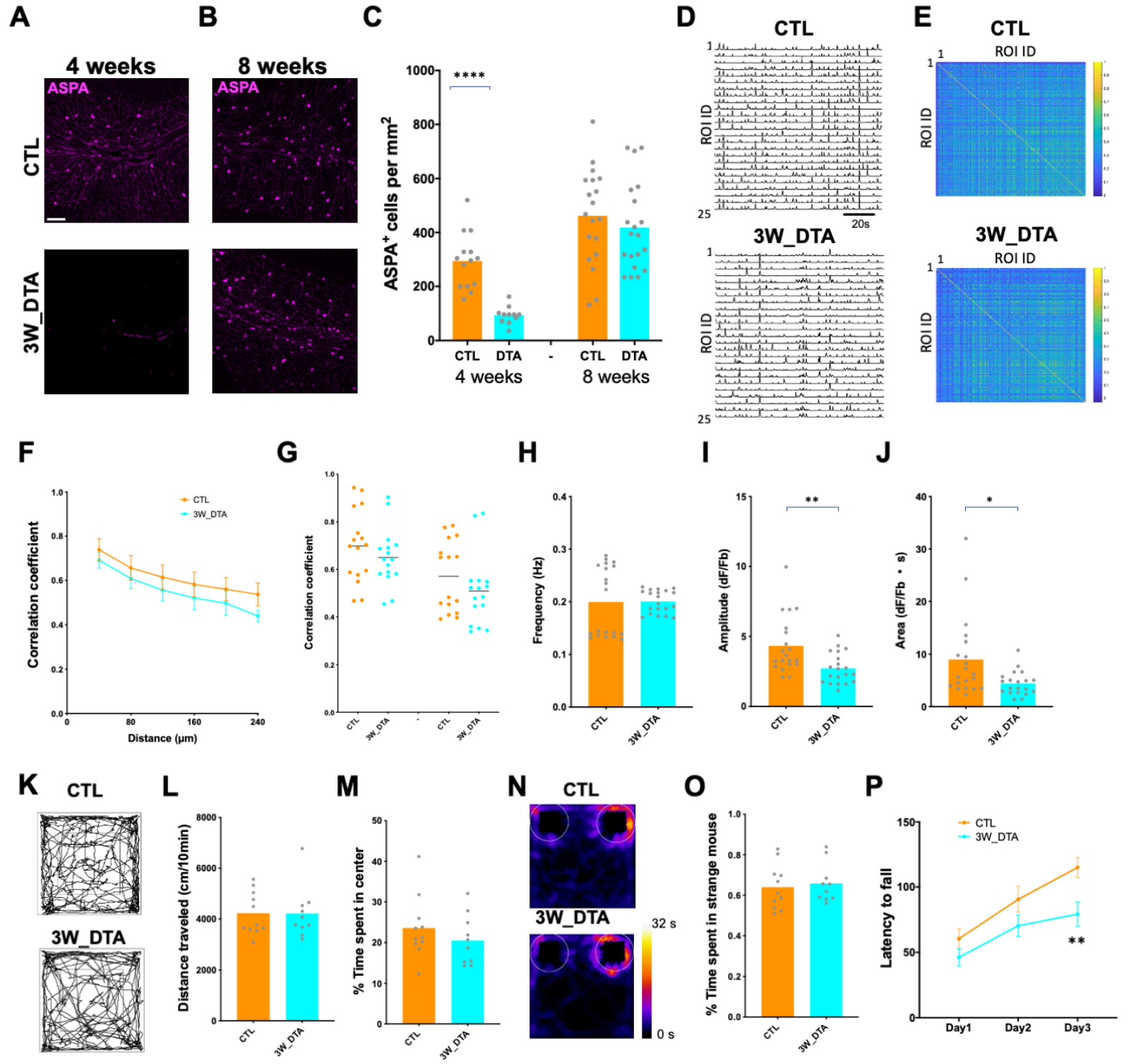
A
B
C
D
E
4 weeks
8 weeks
ASPA
CTL
3W_DTA
ASPA+ cells per mm2
****
CTL
DTA
4 weeks
8 weeks
ROI ID
20s
F
G
H
I
J
Correlation coefficient
Distance (μm)
Frequency (Hz)
Amplitude (dF/Fb)
Area (dF/Fb • s)
**
*
K
L
M
N
O
P
Distance traveled (cm/10min)
% Time spent in center
32 s
0 s
% Time spent in strange mouse
Latency to fall
Day1
Day2
Day3

Fig.6

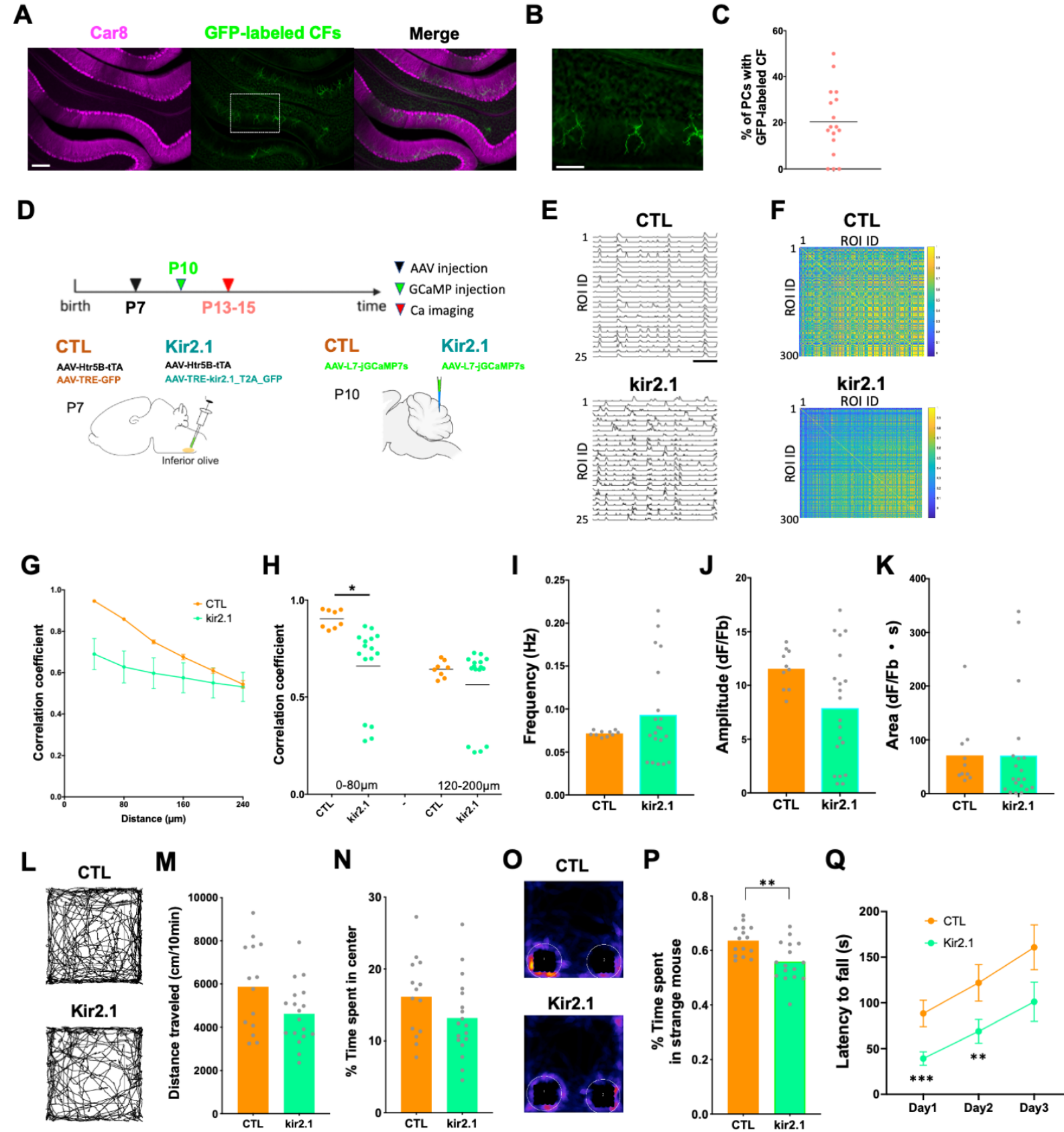
A
Car8
GFP-labeled CFs
Merge
B
C
% of PCs with GFP-labeled CF
D
P10
birth
P7
P13-15
time
AAV injection
GCaMP injection
Ca imaging
CTL
AAV-Htr5B-tTA
AAV-TRE-GFP
Kir2.1
AAV-Htr5B-tTA
AAV-TRE-kir2.1_T2A_GFP
CTL
AAV-L7-jGCaMP7s
Kir2.1
AAV-L7-jGCaMP7s
P7
Inferior olive
P10
E
CTL
ROI ID
kir2.1
F
CTL
ROI ID
kir2.1
G
Correlation coefficient
Distance (μm)
CTL
kir2.1
H
Correlation coefficient
0-80μm
120-200μm
I
Frequency (Hz)
J
Amplitude (dF/Fb)
K
Area (dF/Fb • s)
L
CTL
Kir2.1
M
Distance traveled (cm/10min)
N
% Time spent in center
O
CTL
Kir2.1
P
% Time spent in strange mouse
Q
Latency to fall (s)
Day1
Day2
Day3